

QMugs: Quantum Mechanical Properties of Drug-like Molecules

Clemens Isert^{1,†}, Kenneth Atz^{1,†}, José Jiménez-Luna^{1,2,*}, and Gisbert Schneider^{1,3,*}

¹Department of Chemistry and Applied Biosciences, RETHINK, ETH Zurich, 8093 Zurich, Switzerland.

²Department of Medicinal Chemistry, Boehringer Ingelheim Pharma GmbH & Co. KG, Birkendorfer Straße 65, 88397 Biberach an der Riss, Germany.

³ETH Singapore SEC Ltd, 1 CREATE Way, #06-01 CREATE Tower, Singapore 138602, Singapore.

*corresponding authors: Gisbert Schneider (gisbert@ethz.ch), José Jiménez-Luna (jose.jimenez@rethink.ethz.ch)

†these authors contributed equally to this work

ABSTRACT

Machine learning approaches in drug discovery, as well as in other areas of the chemical sciences, benefit from curated datasets of physical molecular properties. However, there is a lack of sufficiently large data collections that include first-principle quantum chemical information on bioactive molecules, such as single-point electronic properties, quantum mechanical wave functions and density-functional theory (DFT) matrices. The open-access QMugs (Quantum-Mechanical Properties of Drug-like Molecules) dataset fills this void. The QMugs collection comprises quantum mechanical properties of more than 665k biologically and pharmacologically relevant molecules extracted from the ChEMBL database, totaling ~ 2 M conformers. QMugs contains optimized molecular geometries and thermodynamic data obtained via the semi-empirical method GFN2-xTB. Atomic and molecular properties (*e.g.*, partial charges, energies, and rotational constants) are provided on both the GFN2-xTB and on the DFT (ω B97X-D/def2-SVP) levels of theory. QMugs also comprises the respective quantum mechanical wave functions, including DFT density and orbital matrices, totaling over 7 terabytes of uncompressed data. This dataset is intended to facilitate the development of models that learn from molecular data on different levels of theory while also providing insight into the corresponding relationships between molecular structure and biological activity.

Background & Summary

Machine learning methodologies are increasingly becoming well-established tools in many chemistry-related disciplines, such as drug discovery¹, material science², and physical chemistry³. In recent years, significant progress has been made in quantum-based machine learning (QML) methods⁴, which aim to accurately and computationally inexpensively predict the governing properties of atomistic systems, such as energies and forces^{5–12}, dipole moments¹³, wave functions^{14,15} and electron densities^{16,17}. Despite the success and promise surrounding the applicability of such approaches, several challenges remain for QML. Arguably, one of the most important challenges is the increasing need for curated, comprehensive datasets.¹³ While several options, such as the QM9¹⁸ or ANI-1¹⁹ sets have paved the way for the development of current-generation QML methods^{5–8,20–22}, the computational cost entailed in their generation limits both the scope of the explored chemical space (*e.g.*, molecule size, atom-type diversity), and prospective modeling applicability^{13,23}.

There has been a recent surge in interest in the delta-learning (Δ -learning) of chemical properties, which aims to use a machine learning model to predict a physically relevant quantity, such as those generated by density-functional theory (DFT) by utilizing information extracted with a computationally cheaper method^{21,24} (*e.g.*, semi-empirical approaches such as GFN2-xTB^{25–29} and PM6³⁰). Datasets that enable this type of learning are scarce and could promote the development of accurate models at potentially a fraction of the computational cost of more precise alternatives³¹. Furthermore, datasets that provide three-dimensional conformational data, for a wide variety of chemical space, at levels of theory higher than classical force fields^{32,33}, could boost the performance of machine learning methods in predicting properties from ensembles as well as generative models of conformations. Relevant examples include the PubChemQC-PM6²² and GEOM³³ datasets, which include molecules with properties computed using different semi-empirical levels of theory. Finally, there is a clear potential to open up new lines of research by combining biological annotations (*e.g.*, from molecular databases such as ChEMBL³⁴), and additional QM-derived physical information.

This work introduces QMugs (Quantum-Mechanical Properties of Drug-like Molecules), a data collection of over 665k curated molecular structures extracted from the ChEMBL database, with accompanying computed quantum mechanical properties. Different levels of theory were combined in these calculations. Per compound, three conformers were generated,

and their geometries were optimized using the semi-empirical GFN2-xTB method^{25–29}, whereas a comprehensive array of quantum properties was computed at the DFT level of theory using the ω B97X-D functional³⁵ and the def2-SVP Karlsruhe basis set³⁶. The data collection presented herein is put in the context of other sets that also feature DFT-level properties. A descriptive evaluation against QM9¹⁸, PubchemQC³⁷, and the ANI-1¹⁹ datasets is provided in Figure 1B, as well as in Table 1. As previously reported for the ChEMBL database³⁸, most of the considered drug-like molecules in this study fall within the rod-disk axis in the principal moments of inertia plot³⁹ (Figure 1A). Furthermore, the vast majority of the included compounds (~ 641k, 96.3%) were previously unreported in other DFT data collections, while also providing equivalent information at additional levels of theory, namely GFN2-xTB. With an average of 30.6 and a maximum of 100 heavy atoms per compound (Table 1 & Figure 2), QMugs also features molecular samples that are considerably larger than those provided by other datasets. To the best of our knowledge, this work is the first to provide a large and diverse dataset of quantum mechanical wave functions represented as local bases of atomic orbitals (*i.e.*, DFT density and orbital matrices). Single-point properties as well as wave functions were computed with the Psi4 software suite⁴⁰ for all the conformers (~ 2.0M) present in the database, totaling over 7 terabytes of supplied quantum mechanical data.

Overall, the utility of the presented dataset is fourfold: (i) it will provide researchers with the largest-to-date dataset to either directly predict the quantum chemical properties, or learn a property mapping between two popular quantum mechanical levels of theory (*i.e.*, GFN2-xTB and ω B97X-D/def2-SVP); (ii) it will facilitate the development of novel machine-learning methodologies for the generation of molecular conformations and molecular property predictions via their ensembles; (iii) it will enable the development of novel deep learning frameworks for the prediction of the quantum mechanical wave function in a local basis of atomic orbitals from which all ground-state properties as well as electron densities can be derived; and (iv) it will enable research towards the exploration of QML methods quantum featurization in the context of pharmacologically relevant, annotated biological data.

Methods

Molecules were extracted from the ChEMBL database³⁴ (version 27). Conformers were generated using RDKit⁴¹ and GFN2-xTB^{25,26,28,29}. DFT (ω B97X-D/def2-SVP) calculations were carried out via Psi4⁴⁰. A similar approach was adopted in a previous study on transition-metal complexes.¹³ An overview of the data processing pipeline is given in Figure 3, while individual steps are described in more detail in the following subsections.

In chemical terminology, the term “conformation” refers to any arrangement of atoms in space, whereas “conformer” refers to a conformation that is a local minimum on the potential energy surface of the molecule.⁴² In the analyses that follow, the term “conformation” is loosely used to refer to both, unless explicitly mentioned otherwise.

Data extraction and SMILES processing

Single-protein targets with assay information for at least 10 compounds with unique internal identifiers were extracted from the ChEMBL database. Several activity and annotation filters were subsequently applied to these compounds (see ESI for a detailed query description). This procedure resulted in 685,917 molecules with unique external identifiers (ChEMBL-IDs), represented by their Simplified Molecular Input Line Entry Specification (SMILES)⁴³. Molecules were neutralized, and salts and solvents were removed using the ChEMBL Structure Pipeline package^{44,45}. For compounds consisting of multiple separate fragments after this “washing” procedure, all except the one with the highest number of heavy atoms were discarded. Additionally, molecules containing fewer than 3 or more than 100 heavy atoms, as well as radical species and molecules with a net charge different from zero after the attempted neutralization, were removed. Atom types included in the QMugs dataset are hydrogen, carbon, nitrogen, oxygen, fluorine, phosphorus, sulfur, chloride, bromide, and iodine.

Conformer generation and optimization

With the procedure described herein, a compromise between efficient molecular conformational search and practical computational expense considerations was sought.

The RDKit⁴¹ implementation of the Experimental-Torsion Knowledge Distance Geometry (ETKDG) method⁴⁶ was used to generate up to 100 conformers for each molecule, with a maximum of 1000 embedding attempts and an initial coordinate assignment using distance-matrix eigenvalues and default settings (`boxSizeMult=2.0`, `force-field tolerance=1e-3`). Upon no successful conformer generation, it was re-attempted via random assignment of the starting coordinates. The resulting conformers were further minimized using the Merck molecular force field⁴⁷ (MMFF94s) for a maximum of 1000 iterations, with default settings (`nonBondedThresh=100.0`). The lowest-energy conformer (according to the selected force field) for each structure was then used as a starting point for meta-dynamics (MTD) simulations. Stereocenters that were previously undefined in the SMILES extraction procedure were assigned in this conformer generation process.

For each generated conformer, an MTD simulation was performed with the xTB software package²⁸ for a duration of 5 ps with time steps of 1 fs, at a temperature of 300 K. The biasing root-mean-square deviation (RMSD) potential used for all MTD

simulations is given by $E_{\text{bias}}^{\text{RMSD}} = \sum_{i=1}^N k_i \exp(\alpha \Delta_i^2)$, where N is the number of reference structures, k_i the pushing strength, Δ_i the collective variable (*i.e.*, the RMSD between structure i and a reference structure), and α the width of the Gaussian potential used in the RMSD criterion. Simulations were carried out with $\alpha = 1.2 a_0^{-1}$ and $k_i = 0.2 \text{ mE}_h$ with snapshots taken every 50 fs, resulting in 100 conformations stored with their corresponding energies. To obtain conformationally diverse samples, these structures were subsequently clustered into three groups via the k -means⁴⁸ algorithm, as implemented in the scikit-learn⁴⁹ (version 0.23.1) Python package using the pairwise RMSD of the aligned structures as molecular features. The conformation with the lowest-energy value from each cluster was then selected for further processing. The three resulting conformations for each molecule were then optimized using the GFN2-xTB^{25,26,28,29} method using energy and gradient convergence criteria of $5 \times 10^{-6} E_h$ and $1 \times 10^{-3} E_h \alpha^{-1}$, respectively, and the approximate normal coordinate rational function optimizer (ANCopt). Harmonic frequencies, entropies, enthalpies and heat capacities at 298.15 K were extracted at the end of the geometry optimization process. Structures for which vibrational frequencies with imaginary wave numbers were obtained — indicative of failure to reach energy minima — were subjected to additional optimizations until no significant ones remained, up to a maximum of 100 attempts.

Quantum mechanical calculations

Single-point electronic calculations were performed for the optimized geometries using the ω B97X-D quantum functional and the def2-SVP basis set as implemented in the open-source quantum-chemistry software suite Psi4⁴⁰. Single-point properties such as formation and orbital energies, dipole moments, rotational constants, partial charges, bond orders, valence numbers, as well as wave functions including α and β DFT-density matrices, orbital matrices, and the atomic-orbital-to-symmetry-orbital transformer matrix were obtained. For practical reasons, 52 structures whose DFT calculations required computational resources that exceeded empirically determined limits, or for which calculations were unsuccessful, were discarded (see ESI for details).

Data Records

All computed molecular structures, as well as their corresponding properties and wave functions are accessible through the ETH Library Collection service ([Data Citation 1](#))⁵⁰.

Format specification

A `summary.csv` comma-separated file contains computed molecular-level properties and additional annotations. A compressed tarball file (`structures.tar.gz`) of ~ 7 gigabytes (GB) contains plain MDL structure-data files⁵¹ (SDFs) with embedded atomic and molecular properties, grouped in sub-directories according to their respective ChEMBL identifiers. These SDFs include single-point electronic properties calculated on the GFN2-xTB and ω B97X-D/def-SVP levels of theory, as described in Table 2. A second compressed tarball file (`vibspectra.tar.gz`, ~ 3 GB) contains vibrational spectra.

Wave function files, including additional properties such as DFT-density and orbital matrices, as described in Table 3, are split into 100 compressed tarballs (`wfns_xx.tar.gz`) of ~ 50 GB each for easier management and downloading. These are supplied as NumPy⁵² (`.npy`) binary files, which can be read using the Psi4 software package. Molecules (with all conformers grouped together) were assigned at random to the tarballs to enable easy use of subsets of the QMugs dataset without having to download all the files. The assignment of ChEMBL identifiers to tarballs is described in a `tarball_assignment.csv` file.

Technical Validation

Optimized geometry sanity checks

Four consecutive geometry checks were performed to filter out structures for which the geometry optimization procedure converged to unrealistic conformations. To determine suitable thresholds for removing a structure from our dataset, the generated geometries were compared to experimental reference values and to DFT-optimized geometries extracted from the PubChemQC dataset³⁷. Specifically, we investigated (i) the deviation of bond lengths from experimental reference values, (ii) isomorphism between the initial molecular graphs and those obtained after geometry optimization, (iii) linearity of triple bonds, and (iv) planarity of aromatic rings. Structures were removed from the dataset if they failed any test of these tests. In total, 10,986 (0.55%) conformations were discarded from the dataset. Each test is briefly described in the following subsections, with further technical details reported in the ESI.

Deviation of bond lengths from experimental reference values

Bond lengths in the optimized structures were compared to average experimental reference values for bonds of the same bond type (single, double, triple, or aromatic) and between the same atoms. Reference values were obtained from the Computational Chemistry Comparison and Benchmark DataBase (CCCBDB)⁵³, and the largest absolute bond-length deviation from reference

values was recorded per molecule. Bonds for which no reference value was available (0.75%) were omitted. The same analysis was carried out for molecules from the PubChemQC dataset containing the same atom types as QMugs, in order to obtain a comparable set with respect to the present atom types. The PubChemQC set (3,834,382 conformations with reference bond lengths) showed a deviation of 0.06 ± 0.04 Å (median \pm 1 standard deviation), whereas the QMugs dataset (2,004,003 conformations with reference bond lengths) showed a deviation of 0.07 ± 0.03 Å. Based on the observed distribution of bond-length deviations from experimental reference values (Figure S1 in ESI) and manual investigation of example structures, 0.2 Å was determined to be a suitable threshold for a conformation to be removed from the dataset, which included 6,131 (0.31%) examples.

Molecular graph isomorphism

It was investigated whether atom connectivity could be reconstructed after removing bond information from the generated SDFs. To this end, molecular graphs constructed exclusively from atom positions and types were compared to those obtained using the original atom connectivity (see ESI for details). 1,568 (0.08%) conformations for which the resulting molecular graphs were non-isomorphic failed this test.

Deviation of triple bonds from linear geometry

The deviation of triple bonds from their ideal linear geometry was examined. In this investigation, ring triple bonds were not considered owing to routinely-occurring deviations from linear geometry in systems with high ring strain⁵⁴. The largest deviation from a 180° (linear) bond angle was recorded for each molecule containing at least one non-ring triple bond. The same analysis was performed on the PubChemQC dataset³⁷. Triple-bond-containing molecules from PubchemQC and QMugs (273,320 and 165,101 samples, respectively) show deviations of $1.38 \pm 1.46^\circ$ (median \pm 1 standard deviation), and $1.46 \pm 2.13^\circ$, respectively. Based on the observed distribution of triple bond angles from a linear geometry (Figure S2 in ESI) and manual inspection of structures, a 10° deviation was identified as a suitable threshold. 1,147 (0.06%) conformations failed this test.

Deviation of aromatic rings from planar geometry

The planarity of carbon-containing aromatic rings was also investigated. For each molecule containing aromatic carbon atoms, the largest dihedral angle between the two planes spanned by each aromatic carbon atom and its three neighbors was recorded (see ESI for details). The same analysis was performed on the PubChemQC dataset³⁷. Molecules from PubchemQC and QMugs (2,391,589 and 1,950,929 conformations with aromatic carbons, respectively) showed median dihedral angles (\pm 1 standard deviation) of $1.70 \pm 1.85^\circ$ and $2.99 \pm 2.20^\circ$, respectively. Based on the observed distribution of dihedral angles from planar geometries (Figure S3 in ESI) and manual inspection of structures, 2,769 (0.14%) conformations with aromatic carbon dihedral angles above 15° were discarded.

Further geometrical assessment

The changes in the molecular geometries along the applied pipeline were examined in order to evaluate the effects of the applied steps. Figure 4A shows the mean pairwise RMSD of atom positions between the conformations of each molecule at different steps along the pipeline. Conformations sampled during MTD simulations show a mean pairwise RMSD of 2.40 ± 0.52 Å (median \pm 1 standard deviation). The *k*-means clustering procedure accomplishes the envisaged task of sampling conformations with higher geometric diversity (2.67 ± 0.74 Å). During the geometry optimization process, conformational diversity decreases (2.48 ± 0.86 Å). Unsurprisingly, for some molecules featuring rigid structures, conformations tend to converge toward the same energy minimum (0.09 % of molecules show a mean pairwise RMSD < 0.01 Å between their optimized conformers).

The degree to which the molecular geometries changed during the final optimization step was further analyzed. Molecules with initially more diverse conformations (higher mean pairwise RMSD of pre-optimized conformations) were shown to undergo a greater change in atom positions (mean RMSD of pre- vs. post-optimized conformations) during optimization with the GFN2-xTB method (Figure 4B). The observed heteroscedastic behavior of these two properties indicates that while the mean RMSD of pre- vs. post-optimized conformations tends to increase with higher mean pairwise RMSD of pre-optimized conformations, its variance also increases.

Finally, the suitability of GFN2-xTB as a lower-cost surrogate for DFT-level geometry optimization (Figure 4C) was confirmed. 500 randomly-chosen structures prior to semi-empirical geometry optimization from the QMugs dataset were further subjected to DFT-level geometry optimization (ω B97X-D/def2-SVP), discarding structures that could not be converged in 100 iterations or with the computational resources described in the ESI. The RMSDs between the structures independently optimized at both levels of theory were then measured. The pairs of structures show RMSDs of 0.47 ± 0.63 Å (median \pm 1 standard deviation), indicating that the chosen semi-empirical method obtains similar geometries to those obtained with more expensive first-principle calculations. Large RMSDs in some example pairs (Figure 4C) could be interpreted as indicative of convergence to distinct local minima.

For 2,067 molecules, their individual conformations have different SMILES describing two different (*E*)/(*Z*) isomers. Those structures are either α - β -unsaturated ketones, α - β -unsaturated nitriles, imine, or azo compounds, for which isomerization might be plausible^{55,56}. In part due to the applied washing procedure, 17,176 molecules can be represented with a SMILES string that is shared with at least one other ChEMBL-ID.

Validation of single-point properties

To validate the general agreement between the two methods employed in this work, the correlation between a series of single-point properties computed on both levels of theory was analyzed. Both global, molecular (Figure 5) and local, atomic/bond properties (Figures 6 & 7) were considered. All single-point molecular properties showed a high degree of correlation. Formation energies E_{Form} (Figure 5A), which were obtained by subtracting atomic energies E_{Atom} from total internal energies U_{RT} , show a Pearson correlation coefficient (PCC) of 0.998. Dipole moments μ and rotational constants A (excl. 22 small structures with very high rotational constants; Figure 5B,C) display PCCs of 0.969 and 0.999, respectively. Orbital energies, namely the energies for highest occupied (HOMO) E_{HOMO} and lowest unoccupied molecular orbitals (LUMO) E_{LUMO} and HOMO-LUMO gaps E_{Gap} show PCCs of 0.769, 0.924 and 0.830, respectively (Figures 5 D, E & F). The observed PCCs for all six single-point molecular properties indicate good agreement between the two methods. Atom-type-specific partial charges for the 10 atom-types in QMugs (Figure 6, ESI Table 1) as well as the 15 most abundant covalent bonds orders (Figure 7, ESI Table 2) also show high correlations between the two methods used herein. Regarding partial charges, 7 out of the 10 atom types considered in QMugs were observed to have PCCs > 0.8, with the remaining carbon, nitrogen, and oxygen atom-types resulting in lower PCCs of 0.574, 0.124, and 0.274, respectively. Regarding bond orders, 10 out of the 15 show PCCs > 0.9 and 14 out of 15 display PCCs > 0.75 (see ESI Table 2 for additional metrics). Notably only carbon-fluorine bonds display a larger discrepancy between both levels of theory, with an observed PCC of 0.153. The observed correlations in both molecular and atomic single-point properties between GFN2-xTB and ω B97X-D/def2-SVP confirm the suitability of the former method as a computationally affordable starting point for Δ -learning of DFT-level properties.

Usage Notes

All data files can be accessed via any modern web browser, and can be programmatically downloaded using the provided instructions in the archive's readme. The provided SDFs can be processed using standard cheminformatics software (e.g., RDKit⁴¹, KNIME⁵⁷), and wave function files using the Psi4⁴⁰ software package or directly using Numpy⁵².

Code availability

All analyses were supported by the Python programming language (version 3.7.7) and its scientific software stack⁵². Molecular conformations were generated using RDKit⁴¹ (version 2020.03.3) and GFN2-xTB²⁵⁻²⁹ (version 6.3.1). All quantum mechanical calculations were carried out with Psi4⁴⁰ (version 1.3.2). Molecular structure visualizations were created using PyMol⁵⁸ (version 2.3.5) and ChemDraw (version 19.1.1.32). The rclone (<https://rclone.org>) WebDAV client was used for all data uploading purposes.

Acknowledgements

We thank Dr. Jan A. Hiss and Dr. Petra Schneider for their valuable insights and discussions. Special thanks to Andreas la Roi from the ETH Research Collection team and to the ETH cluster team for their technical support throughout this project. This work was financially supported by the ETH RETHINK initiative, the Swiss National Science Foundation (grant no. 205321_182176), and Boehringer Ingelheim Pharma GmbH & Co. KG. C.I. acknowledges support from the Scholarship Fund of the Swiss Chemical Industry.

Author contributions statement

Clemens Isert: Methodology, Formal Analyses, Writing. **Kenneth Atz:** Methodology, Formal Analyses, Writing. **José Jiménez-Luna:** Conceptualization, Methodology, Writing. **Gisbert Schneider:** Supervision, Writing.

Competing interests

G.S. is a cofounder of inSili.com LLC, Zurich, and a consultant to the pharmaceutical industry.

References

1. Gawehn, E., Hiss, J. A. & Schneider, G. Deep learning in drug discovery. *Mol. Inform.* **35**, 3–14 (2016).
2. Schmidt, J., Marques, M. R., Botti, S. & Marques, M. A. Recent advances and applications of machine learning in solid-state materials science. *Npj Comput. Mater.* **5**, 1–36 (2019).
3. Von Lilienfeld, O. A. Quantum machine learning in chemical compound space. *Angew. Chem. Int. Ed.* **57**, 4164–4169 (2018).
4. von Lilienfeld, O. A., Müller, K.-R. & Tkatchenko, A. Exploring chemical compound space with quantum-based machine learning. *Nat. Rev. Chem.* **4**, 347–358 (2020).
5. Satorras, V. G., Hoogeboom, E. & Welling, M. E-(n) equivariant graph neural networks. *arXiv preprint arXiv:2102.09844* (2021).
6. Schütt, K. T., Unke, O. T. & Gastegger, M. Equivariant message passing for the prediction of tensorial properties and molecular spectra. *arXiv preprint arXiv:2102.03150* (2021).
7. Huang, B. & von Lilienfeld, O. A. Quantum machine learning using atom-in-molecule-based fragments selected on the fly. *Nat. Chem.* **12**, 945–951 (2020).
8. Christensen, A. S., Bratholm, L. A., Faber, F. A. & Anatole von Lilienfeld, O. FCHL revisited: Faster and more accurate quantum machine learning. *J. Chem. Phys.* **152**, 044107 (2020).
9. Heinen, S., von Rudorff, G. F. & von Lilienfeld, O. A. Quantum based machine learning of competing chemical reaction profiles. *arXiv preprint arXiv:2009.13429* (2020).
10. Heinen, S., Schwilk, M., von Rudorff, G. F. & von Lilienfeld, O. A. Machine learning the computational cost of quantum chemistry. *Mach. Learn. Sci. Technol.* **1**, 025002 (2020).
11. Christensen, A. S., Faber, F. A. & von Lilienfeld, O. A. Operators in quantum machine learning: Response properties in chemical space. *J. Chem. Phys.* **150**, 064105 (2019).
12. Faber, F. A., Christensen, A. S., Huang, B. & Von Lilienfeld, O. A. Alchemical and structural distribution based representation for universal quantum machine learning. *J. Chem. Phys.* **148**, 241717 (2018).
13. Balcells, D. & Skjelstad, B. B. tmQM dataset — quantum geometries and properties of 86k transition metal complexes. *J. Chem. Inf. Model.* **60**, 6135–6146 (2020).
14. Unke, O. T. *et al.* SE(3)-equivariant prediction of molecular wavefunctions and electronic densities (2021). [2106.02347](https://arxiv.org/abs/2106.02347).
15. Schütt, K., Gastegger, M., Tkatchenko, A., Müller, K.-R. & Maurer, R. J. Unifying machine learning and quantum chemistry with a deep neural network for molecular wavefunctions. *Nat. Commun.* **10**, 1–10 (2019).
16. Grisafi, A. *et al.* Transferable machine-learning model of the electron density. *ACS Cent. Sci.* **5**, 57–64 (2018).
17. Fabrizio, A., Grisafi, A., Meyer, B., Ceriotti, M. & Corminboeuf, C. Electron density learning of non-covalent systems. *Chem. Sci.* **10**, 9424–9432 (2019).
18. Ramakrishnan, R., Dral, P. O., Rupp, M. & Von Lilienfeld, O. A. Quantum chemistry structures and properties of 134 kilo molecules. *Sci. Data* **1**, 1–7 (2014).
19. Smith, J. S., Isayev, O. & Roitberg, A. E. ANI-1, a data set of 20 million calculated off-equilibrium conformations for organic molecules. *Sci. Data* **4**, 170193 (2017).
20. Smith, J. S., Isayev, O. & Roitberg, A. E. ANI-1: An extensible neural network potential with DFT accuracy at force field computational cost. *Chem. Sci.* **8**, 3192–3203 (2017).
21. Smith, J. S. *et al.* The ANI-1ccx and ANI-1x data sets, coupled-cluster and density functional theory properties for molecules. *Sci. Data* **7**, 1–10 (2020).
22. Nakata, M., Shimazaki, T., Hashimoto, M. & Maeda, T. PubChemQC PM6: Data sets of 221 million molecules with optimized molecular geometries and electronic properties. *J. Chem. Inf. Model.* **60**, 5891–5899 (2020).
23. Glavatskikh, M., Leguy, J., Hunault, G., Cauchy, T. & Da Mota, B. Dataset’s chemical diversity limits the generalizability of machine learning predictions. *J. Cheminformatics* **11**, 1–15 (2019).
24. Qiao, Z., Welborn, M., Anandkumar, A., Manby, F. R. & Miller III, T. F. Orbnet: Deep learning for quantum chemistry using symmetry-adapted atomic-orbital features. *J. Chem. Phys.* **153**, 124111 (2020).

25. Grimme, S., Bannwarth, C. & Shushkov, P. A robust and accurate tight-binding quantum chemical method for structures, vibrational frequencies, and noncovalent interactions of large molecular systems parametrized for all spd-block elements ($Z=1-86$). *J. Chem. Theory Comput.* **13**, 1989–2009 (2017).
26. Bannwarth, C., Ehlert, S. & Grimme, S. GFN2-xTB—An accurate and broadly parametrized self-consistent tight-binding quantum chemical method with multipole electrostatics and density-dependent dispersion contributions. *J. Chem. Theory Comput.* **15**, 1652–1671 (2019).
27. Pracht, P., Caldeweyher, E., Ehlert, S. & Grimme, S. A robust non-self-consistent tight-binding quantum chemistry method for large molecules. *Under Review* <https://doi.org/10.26434/chemrxiv.8326202.v1> (2019).
28. Grimme, S. Exploration of chemical compound, conformer, and reaction space with meta-dynamics simulations based on tight-binding quantum chemical calculations. *J. Chem. Theory Comput.* **15**, 2847–2862 (2019).
29. Bannwarth, C. *et al.* Extended tight-binding quantum chemistry methods. *WIREs Comput. Mol. Sci.* **11**, e1493 (2021).
30. Rezac, J., Fanfrlik, J., Salahub, D. & Hobza, P. Semiempirical quantum chemical PM6 method augmented by dispersion and h-bonding correction terms reliably describes various types of noncovalent complexes. *J. Chem. Theory Comput.* **5**, 1749–1760 (2009).
31. Folmsbee, D. & Hutchison, G. Assessing conformer energies using electronic structure and machine learning methods. *Int. J. Quantum Chem.* **121**, e26381 (2021).
32. Bolton, E. E., Kim, S. & Bryant, S. H. PubChem3D: Conformer generation. *J. Cheminformatics* **3**, 1–16 (2011).
33. Axelrod, S. & Gomez-Bombarelli, R. Geom: Energy-annotated molecular conformations for property prediction and molecular generation. *arXiv preprint arXiv:2006.05531* (2020).
34. Mendez, D. *et al.* ChEMBL: Towards direct deposition of bioassay data. *Nucleic Acids Res.* **47**, D930–D940 (2019).
35. Chai, J.-D. & Head-Gordon, M. Long-range corrected hybrid density functionals with damped atom–atom dispersion corrections. *Phys. Chem. Chem. Phys.* **10**, 6615–6620 (2008).
36. Weigend, F. & Ahlrichs, R. Balanced basis sets of split valence, triple zeta valence and quadruple zeta valence quality for h to m: Design and assessment of accuracy. *Phys. Chem. Chem. Phys.* **7**, 3297–3305 (2005).
37. Nakata, M. & Shimazaki, T. PubChemQC project: A large-scale first-principles electronic structure database for data-driven chemistry. *J. Chem. Inf. Model.* **57**, 1300–1308 (2017).
38. Meyers, J., Carter, M., Mok, N. Y. & Brown, N. On the origins of three-dimensionality in drug-like molecules. *Future Med. Chem.* **8**, 1753–1767 (2016).
39. Sauer, W. H. & Schwarz, M. K. Molecular shape diversity of combinatorial libraries: A prerequisite for broad bioactivity. *J. Chem. Inf. Comput. Sci.* **43**, 987–1003 (2003).
40. Smith, D. G. *et al.* Psi4 1.4: Open-source software for high-throughput quantum chemistry. *J. Chem. Phys.* **152**, 184108 (2020).
41. Landrum, G. RDKit: Open-source cheminformatics. <http://www.rdkit.org> (Accessed Sept. 2020).
42. Moss, G. *et al.* Basic terminology of stereochemistry (IUPAC recommendations 1996). *Pure Appl. Chem.* **68**, 2193–2222 (1996).
43. Weininger, D. SMILES, a chemical language and information system. 1. Introduction to methodology and encoding rules. *J. Chem. Inf. Comput. Sci.* **28**, 31–36 (1988).
44. Bento, A. P. *et al.* An open source chemical structure curation pipeline using RDKit. *Under Review* <https://doi.org/10.21203/rs.3.rs-34715/v1> (2020).
45. Bento, A. P. *et al.* ChEMBL Structure Pipeline, v 1.0.0. https://github.com/chembl/ChEMBL_Structure_Pipeline (2020).
46. Riniker, S. & Landrum, G. A. Better informed distance geometry: Using what we know to improve conformation generation. *J. Chem. Inf. Model.* **55**, 2562–2574 (2015).
47. Tosco, P., Stiefl, N. & Landrum, G. Bringing the MMFF force field to the RDKit: Implementation and validation. *J. Cheminformatics* **6**, 37 (2014).
48. Lloyd, S. Least squares quantization in PCM. *IEEE Transactions on Inf. Theory* **28**, 129–137 (1982).
49. Pedregosa, F. *et al.* Scikit-learn: Machine learning in Python. *J. Mach. Learn. Res.* **12**, 2825–2830 (2011).
50. Isert, C., Atz, K., Jiménez-Luna, J. & Schneider, G. QMugs: Quantum Mechanical Properties of Drug-like Molecules. <https://doi.org/10.3929/ethz-b-000482129> (2021).

51. Dalby, A. *et al.* Description of several chemical structure file formats used by computer programs developed at Molecular Design Limited. *J. Chem. Inform. Comput. Sci.* **32**, 244–255 (1992).
52. Harris, C. R. *et al.* Array programming with NumPy. *Nature* **585**, 357–362 (2020).
53. NIST Standard Reference Database 101. Computational Chemistry Comparison and Benchmark DataBase, Release 21, August 2020. <https://cccbdb.nist.gov/expbondlengths1.asp>.
54. Bach, R. D. Ring strain energy in the cyclooctyl system. the effect of strain energy on [3 + 2] cycloaddition reactions with azides. *J. Am. Chem. Soc.* **131**, 5233–5243 (2009).
55. Goulet-Hanssens, A. *et al.* Electrocatalytic Z/E isomerization of azobenzenes. *J. Am. Chem. Soc.* **139**, 335–341 (2017).
56. Roca-Lopez, D., Tejero, T. & Merino, P. DFT investigation of the mechanism of E/Z isomerization of nitrones. *J. Org. Chem.* **79**, 8358–8365 (2014).
57. Berthold, M. R. *et al.* KNIME: The Konstanz Information Miner. In *Studies in Classification, Data Analysis, and Knowledge Organization (GfKL 2007)* (Springer, 2007).
58. Schrödinger LLC. The PyMOL Molecular Graphics System, Version 2.3.5.
59. M. Nakata, T. Maeda, T. Shimazaki, M. Hashimoto. The PubChemQC Project. <http://pubchemqc.riken.jp/> Accessed Sept. 2020.

Figures & Tables

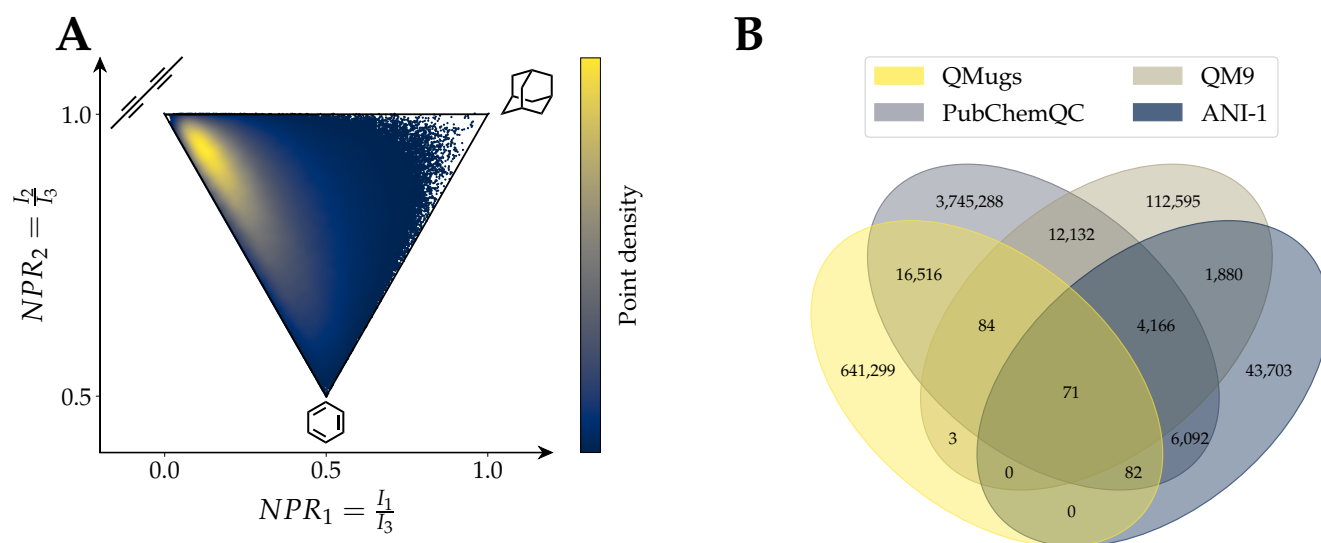


Figure 1. **A)** Principal-moments-of-inertia plot³⁹ for molecules in the QMugs dataset. $NPR_x = x$ -th normalized principal moment, $I_x = x$ -th smallest principal moment of inertia. **B)** Venn diagram showing overlap between QMugs and other well-known datasets with DFT-level computed properties: QM9¹⁸, PubChemQC³⁷, and ANI-1¹⁹. Overlap was computed based on the uniqueness of the InChI representations of the contained molecules. Numbers do not add up to those reported in Table 1 because of InChI strings that occur multiple times.

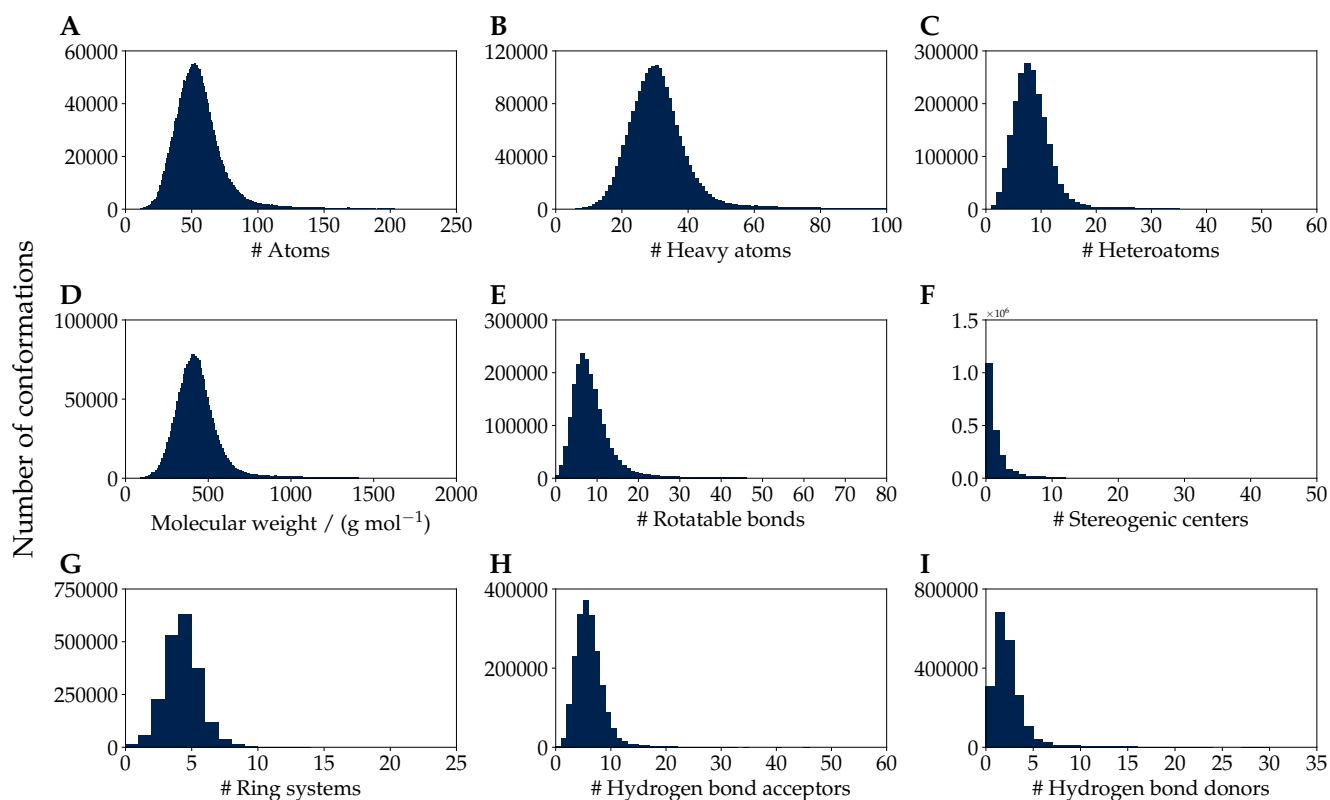


Figure 2. Distribution of properties for the molecules contained in the QMugs dataset.

Table 1. Descriptive statistics of the dataset reported herein in the context of other DFT-level molecular datasets and the information provided by each. The number of molecules for PubChemQC corresponds to that available on the website of the project.⁵⁹ Heavy atom averages are weighted by the number of conformations.

Dataset	Unique compounds	Total conformations	Heavy atoms max (mean)	Method	Δ -learning possible	Wave functions
QM9	133,885	133,885	9 (8.8)	B3LYP/6-31G(2df,p)	✗	✗
ANI-1	57,462	22,057,374	8 (7.1)	ω B97X/6-31G(d)	✗	✗
PubChemQC	3,982,436	3,982,436	51 (14.1)	B3LYP/6-31G(d)	✗	✗
QMugs	665,911	1,992,984	100 (30.6)	GFN2-xTB + ω B97X-D/def2-SVP	✓	✓

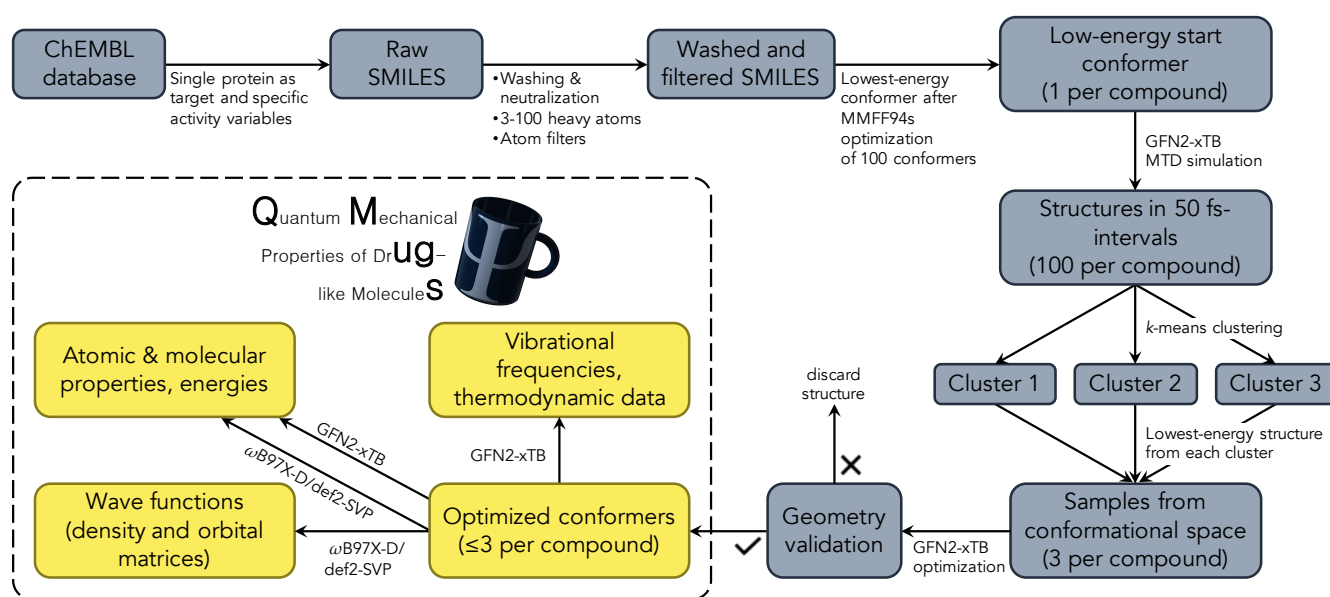


Figure 3. Overview of the data generation process. Molecules were extracted from the ChEMBL database, standardized, and filtered, and starting conformers were generated using the RDKit software package. Metadynamics (MTD) simulations were performed using the GFN2-xTB semi-empirical method to generate three diverse conformations before final geometry optimization. Molecules that did not pass a series of geometric sanity checks were removed. DFT-level properties (ω B97X-D/def2-SVP) were computed using the Psi4 software.

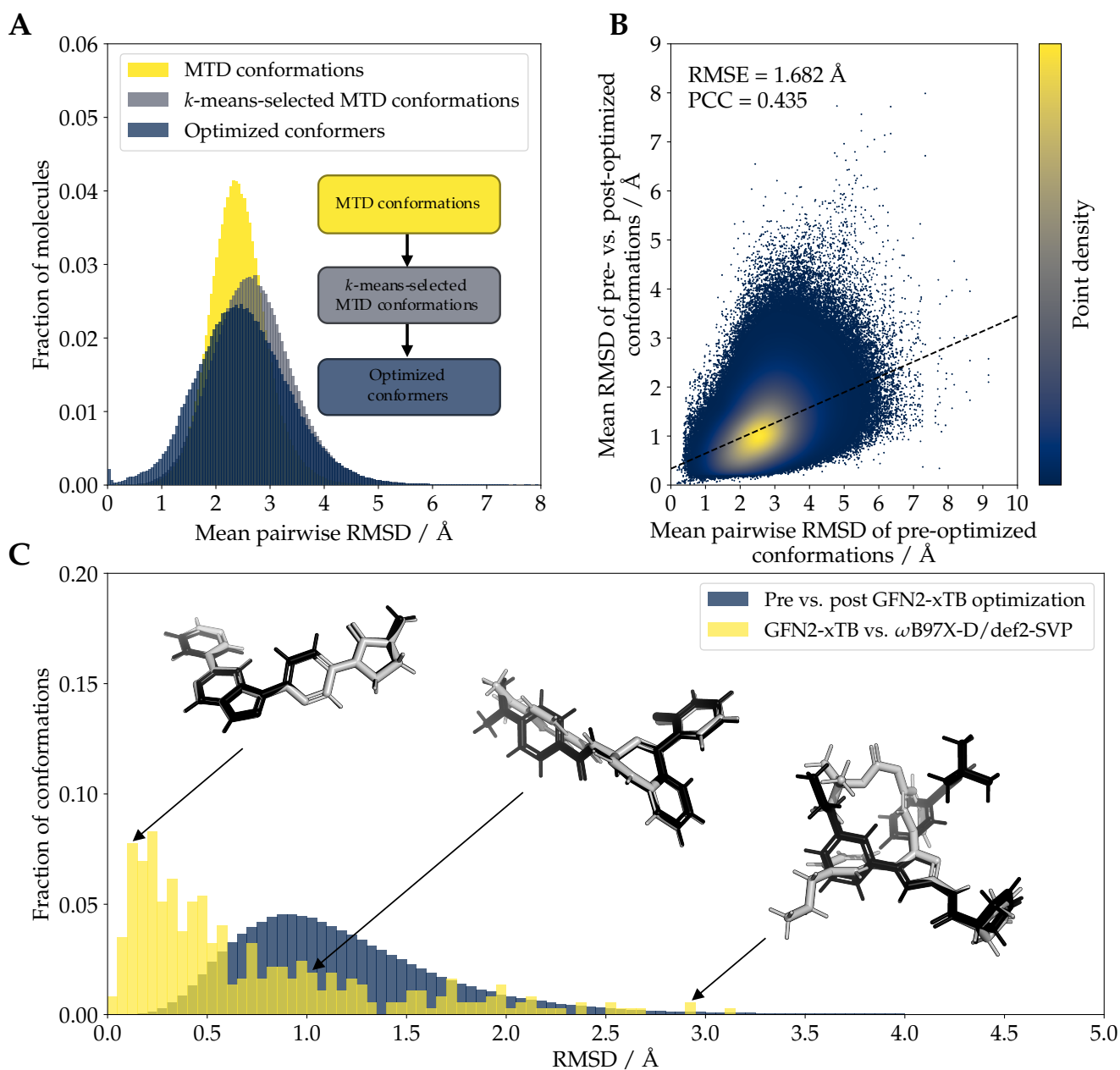


Figure 4. (A) Distributions of mean pairwise RMSD of atom positions between conformations of each molecule in the QMugs dataset at different stages along the pipeline. While the *k*-means sampling process selects conformations that are, on average, more geometrically diverse than the average pair of structures generated by MTD simulations, geometry optimization reduces the geometrical diversity between the optimized conformers. (B) Change in atom positions during geometry optimization vs. mean pairwise RMSD of conformations before optimization. Molecules with initially more diverse conformations displayed a greater change in atom positions than those with initially less diverse conformations. (C) Distribution of RMSD of structures prior to and after optimization with the semi-empirical GFN2-xTB method, and of structures optimized with the same approach vs. with ω B97X-D/def2-SVP. The structures of three molecules with varying differences between the two methods are shown as illustrative examples (black and gray correspond to GFN2-xTB and ω B97X-D/def2-SVP-optimized structures, respectively). For illustrative purposes, the example molecules are aligned on their substructures.

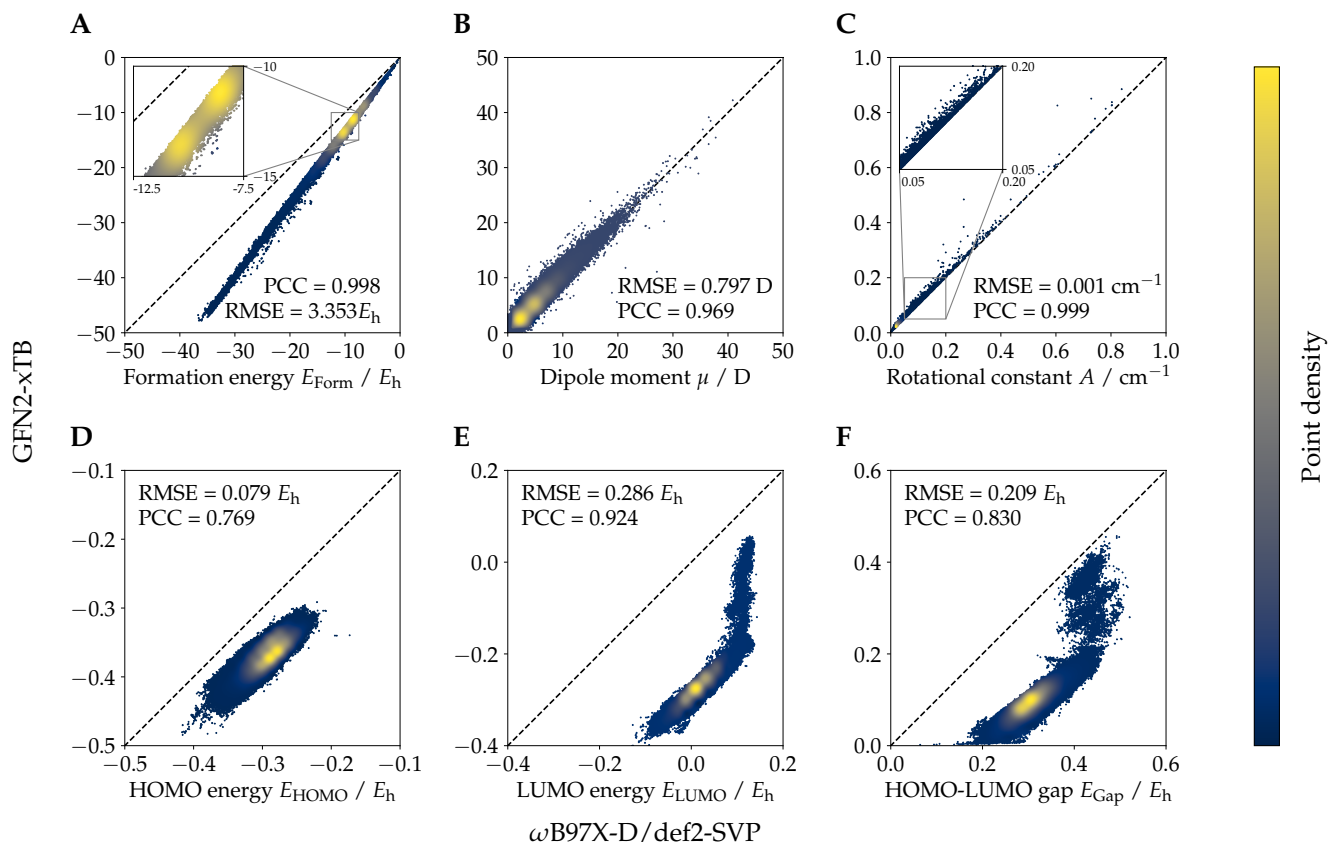


Figure 5. Comparison of molecular properties computed at the two levels of theory considered herein (GFN2-xTB, ω B97X-D/def2-SVP) for the molecules contained in QMugs. The molecular formation energy E_{form} in (A) was calculated by subtracting the atomic U_{Atom} contributions from the total molecular energies U_{RT} . Only the rotational constants A are shown in (C) as their B and C counterparts showed highly similar values. 22 conformations of small molecules show very large rotational constants and are not shown. RMSE and PCC for rotational constant A are 845.834 cm^{-1} and 0.091 respectively, if those structures are included. Abbreviations: RMSE, root mean squared error; PCC, Pearson's correlation coefficient.

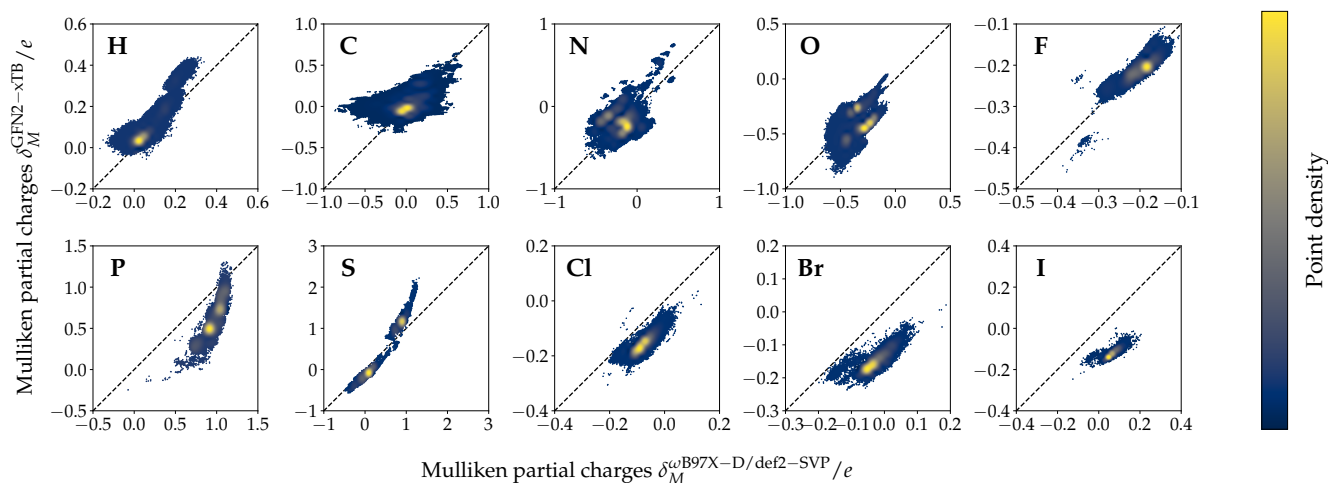


Figure 6. Atom-type-specific partial charge correlations (GFN2-xTB, ω B97X-D/def2-SVP) for the QMugs dataset (see ESI Table 1 for additional metrics)

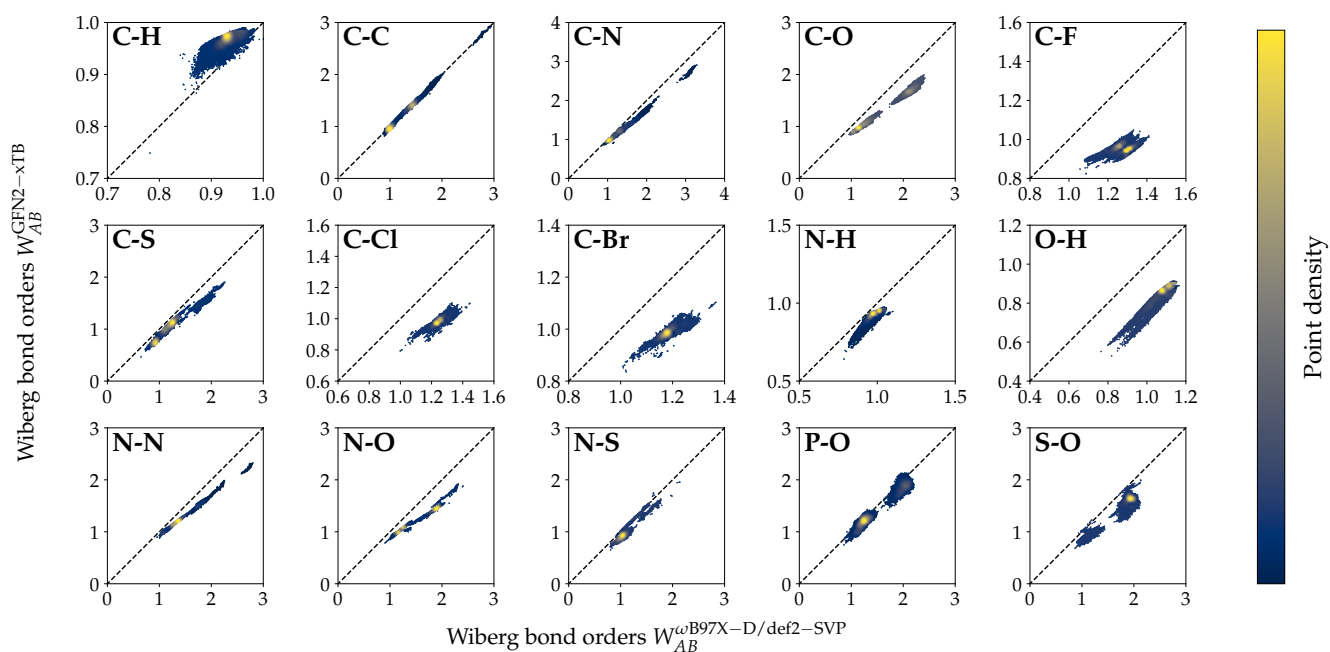


Figure 7. Comparison of Wiberg bond orders between GFN2-xTB and ω B97X-D/def2-SVP for the 15 most frequently occurring bond types in the QMugs dataset. The latter level of theory uses Löwdin-orthogonalization. See ESI Table 2 for additional metrics. For bond types which occurred $> 1\text{M}$ times in the dataset, a randomly chosen sample of 1M bonds is plotted.

Table 2. Calculated properties as stored in the SDFs of the QMugs data collection. Abbreviations: a.u., atomic units; vib., vibrational; rot., rotational; transl., translational. Properties that enable Δ machine learning are labelled with \blacklozenge .

Property	Symbol	Unit	Key	Δ -ML
ChEMBL identifier	-	-	CHEMBL_ID	
Conformer identifier	-	-	CONF_ID	
Total energy	U_{RT}	E_h	GFN2:TOTAL_ENERGY	\blacklozenge
Internal atomic energy	E_{Atom}	E_h	GFN2:ATOMIC_ENERGY	
Formation energy	E_{Form}	E_h	GFN2:FORMATION_ENERGY	\blacklozenge
Total enthalpy	H_{RT}	E_h	GFN2:TOTAL_ENTHALPY	
Total free energy	G_{RT}	E_h	GFN2:TOTAL_FREE_ENERGY	
Dipole (x, y, z, total)	μ	D	GFN2:DIPOLE	\blacklozenge
Quadrupole (xx, xy, yy, xz, yz, zz)	Q_{ij}	D \AA	GFN2:QUADRUPOLE	
Rotational constants (A, B, C)	A, B, C	cm^{-1}	GFN2:ROT_CONSTANTS	\blacklozenge
Enthalpy (vib., rot., transl., total)	ΔH	cal mol^{-1}	GFN2:ENTHALPY	
Heat capacity (vib., rot., transl., total)	C_V	$\text{cal K}^{-1} \text{mol}^{-1}$	GFN2:HEAT_CAPACITY	
Entropy (vib., rot., transl., and total)	ΔS	$\text{cal K}^{-1} \text{mol}^{-1}$	GFN2:ENTROPY	
HOMO energy	E_{HOMO}	E_h	GFN2:HOMO_ENERGY	\blacklozenge
LUMO energy	E_{LUMO}	E_h	GFN2:LUMO_ENERGY	\blacklozenge
HOMO-LUMO gap	E_{Gap}	E_h	GFN2:HOMO_LUMO_GAP	\blacklozenge
Fermi level	E_{Fermi}	E_h	GFN2:FERMI_LEVEL	
Mulliken partial charges	δ_M	e	GFN2:MULLIKEN_CHARGES	\blacklozenge
Covalent coordination number	N_{coord}	-	GFN2:COVALENT_COORDINATION_NUMBER	
Molecular dispersion coefficient	C_6	a.u.	GFN2:DISPERSION_COEFFICIENT_MOLECULAR	
Atomic dispersion coefficients	C_6	a.u.	GFN2:DISPERSION_COEFFICIENT_ATOMIC	
Molecular polarizability	$\alpha(0)$	a.u.	GFN2:POLARIZABILITY_MOLECULAR	
Atomic polarizabilities	$\alpha(0)$	a.u.	GFN2:POLARIZABILITY_ATOMIC	
Wiberg bond orders	M_{AB}	-	GFN2:WIBERG_BOND_ORDER	\blacklozenge
Total Wiberg bond orders	$\sum_{A(A \neq B)} M_{AB}$	-	GFN2:TOTAL_WIBERG_BOND_ORDER	\blacklozenge
Total energy	U_{RT}	E_h	DFT:TOTAL_ENERGY	\blacklozenge
Total internal atomic energy	E_{Atom}	E_h	DFT:ATOMIC_ENERGY	
Formation energy	E_{Form}	E_h	DFT:FORMATION_ENERGY	\blacklozenge
Electrostatic potential	V_{ESP}	V	DFT:ESP_AT_NUCLEI	
Löwdin partial charges	δ_L	e	DFT:LOWDIN_CHARGES	
Mulliken partial charges	δ_M	e	DFT:MULLIKEN_CHARGES	\blacklozenge
Rotational constants (A, B, C)	A, B, C	cm^{-1}	DFT:ROT_CONSTANTS	\blacklozenge
Dipole (x, y, z, total)	μ	D	DFT:DIPOLE	
Exchange correlation energy	\hat{V}_{eN}	E_h	DFT:XC_ENERGY	
Nuclear repulsion energy	\hat{V}_{eN}	E_h	DFT:NUCLEAR_REPULSION_ENERGY	
One-electron energy	\hat{T}_e	E_h	DFT:ONE_ELECTRON_ENERGY	
Two-electron energy	\hat{V}_{ee}	E_h	DFT:TWO_ELECTRON_ENERGY	
HOMO energy	E_{HOMO}	E_h	DFT:HOMO_ENERGY	\blacklozenge
LUMO energy	E_{LUMO}	E_h	DFT:LUMO_ENERGY	\blacklozenge
HOMO-LUMO gap	E_{Gap}	E_h	DFT:HOMO_LUMO_GAP	\blacklozenge
Mayer bond orders	M_{AB}	-	DFT:MAYER_BOND_ORDER	
Wiberg-Löwdin bond orders	W_{AB}	-	DFT:WIBERG_LOWDIN_BOND_ORDER	\blacklozenge
Total Mayer bond orders	$\sum_{A(A \neq B)} M_{AB}$	-	DFT:TOTAL_MAYER_BOND_ORDER	
Total Wiberg-Löwdin bond orders	$\sum_{A(A \neq B)} W_{AB}$	-	DFT:TOTAL_WIBERG_LOWDIN_BOND_ORDER	\blacklozenge

Table 3. Calculated molecular properties stored in the wave function files provided in the QMugs data collection. Mayer and Wiberg-Löwdin bond orders included here represent a superset of the bond orders in the SDFs which additionally comprise bond orders for non-covalent bonds.

Property	Symbol	Key
Alpha density matrix	D_α	matrix, Ca
Beta density matrix	D_β	matrix, Cb
Alpha orbitals	C_α	matrix, Da
Beta orbitals	C_β	matrix, Db
Atomic-orbital-to-symmetry-orbital transformer	C_{AOTOSO}	matrix, aotoso
Mayer bond orders	M_{AB}	MAYER_INDICES
Wiberg-Löwdin bond orders	W_{AB}	WIBERG_LOWDIN_INDICES

QMugs: Quantum Mechanical Properties of Drug-like Molecules

Supporting Information

Clemens Isert^{1,†}, Kenneth Atz^{1,†}, José Jiménez-Luna^{1,2,*}, and Gisbert Schneider^{1,3,*}

¹Department of Chemistry and Applied Biosciences, RETHINK, ETH Zurich, 8093 Zurich, Switzerland.

²Department of Medicinal Chemistry, Boehringer Ingelheim Pharma GmbH & Co. KG, Birkendorfer Straße 65, 88397 Biberach an der Riss, Germany.

³ETH Singapore SEC Ltd, 1 CREATE Way, #06-01 CREATE Tower, Singapore 138602, Singapore.

*corresponding authors: Gisbert Schneider (gisbert@ethz.ch), José Jiménez-Luna (jose.jimenez@rethink.ethz.ch)

†these authors contributed equally to this work

1 Overlap with other datasets

The overlap between the compounds included in the QMugs dataset with those included in other datasets featuring DFT-properties, namely QM9¹, PubchemQC² and ANI-1³, was investigated. Overlap was computed based on the respective compounds' InChI⁴ strings. For each dataset, the molecules were converted from their original formats (QMugs: `.sdf`, QM9: `.xyz`, PubChemQC: `.mol`, ANI-1: SMILES⁵, as obtained with the `pyanitools` module included in the ANI-1 repository) to InChIs using Openbabel^{6,7} (version 3.1.1). Molecules that could not be successfully converted were skipped. The Venn diagram (Fig. 4, main article) was constructed using the `pyvenn`⁸ package. Note that due to different washing procedures, the same compound identifier may refer to different InChI strings in different datasets (*e.g.*, protonated and unprotonated).

2 ChEMBL SQL query

A locally-downloaded MySQL instance of the ChEMBL27 database⁹ (version 8.0.19) was queried¹⁰. Our data extraction procedure is performed in two steps: First, a list of biological targets was extracted. Second, compounds for which a specific activity towards any of these targets was annotated were extracted. Both steps are described in the following.

2.1 Extraction of targets

"Single-protein" targets were selected, for which `activity.standard_types` were reported either as `IC50`, `EC50`, `Ki`, `K`, `Kb`, `Ka`, `Kd`, `Ke`, or `Km` and in units of nM, or as a set of other `activity.standard_types` (*e.g.*, `-log K`) and without units. The following types of annotations were excluded: Annotations with an `assay.relationship_type` other than "homologous" or "direct", annotations with an `assay.confidence_score` below 7, annotations with assay descriptions for mutant species, annotations for potential activity duplicates, annotations with assay data validity comments other than "Manually validated" or "null", and annotations with `activity.activity_comments` indicating missing data such as "Not Determined" or "Not tested". Only targets which had annotations for 10 or more unique compounds (as identified by their `activity.molregno` identifier) after this data extraction process were kept.

2.2 Extraction of compounds

For each of the targets extracted in the previous steps, we queried the SQL database for activity annotations. Annotations for which the `activity.standard_value` or the `activity.standard_unit` was missing were discarded. All `activity.standard_values` for annotations were converted to negative decadic logarithm scales (pX) and values below -3 on this scale were corrected to their absolute value. The `activity.standard_values` for annotations with activity comments denoting inactivity were set to 3 on this log-scale. Annotations where the converted `activity.standard_value` lay outside the range of 3-12 were excluded. For each of the compounds that remained, we extracted the ChEMBL-ID and the canonical SMILES.

3 SMILES filtering

The molecules extracted from the ChEMBL database were filtered to exclude the following SMARTS patterns using RDKit¹¹ (version 2020.03.3.0):

```
B, [*]~P(~[*])(~[*])(~[*])~[*], [*]~S(~[*])(~[*])(~[*])~[*], [S+^3], [P+^3],
[*]~[F,Cl,Br,I]~[*], [Be], [Na], [Al], [Si], [Sc], [Ti], [V], [Cr], [Mn], [Fe], [Co], [Ni], [Cu],
[Zn], [Ga], [Ge], [As], [Se], [Rb], [Sr], [Y], [Zr], [Nb], [Mo], [Tc], [Ru], [Rh], [Pd], [Ag], [Cd],
[In], [Sn], [Sb], [Te], [Cs], [Ba], [La], [Ce], [Pr], [Nd], [Pm], [Sm], [Eu], [Gd], [Tb], [Dy], [Ho],
[Er], [Tm], [Yb], [Lu], [Hf], [Ta], [W], [Re], [Os], [Ir], [Pt], [Au], [Hg], [Pb], [Bi], [Fr]
```

Compounds containing these substructures were excluded as they were either incompatible with the used MMFF94s force field¹² (e.g., B), contained halogens bound to two neighbors (e.g., `[*]~[F,Cl,Br,I]~[*]`), or elements with reduced relevance for drug-like molecules.

4 Computational resources

For practical reasons, molecules whose DFT-calculations demanded computational resources that exceeded empirically determined limits, were discarded. These limits include a maximum processing power of 4 CPU cores for 24 h wall-time, up to 40 GB of system memory, and 100 GB of scratch space. For the single-point property calculations, this was the case for 9 structures. Additionally, 19 structures (GFN2-xTB) and 24 structures (DFT) were discarded as the respective calculations could not be completed successfully.

5 Optimized geometry sanity checks

We performed four consecutive geometry checks (Sections 5.1 – 5.4) to filter out structures for which geometry optimization had converged to unrealistic conformations. Structures failing any of these tests were removed from the dataset. Note that stated numbers of investigated molecules for the QMugs dataset are larger than the size of the final dataset, as only molecules that passed all geometry checks were included in the final dataset. Note that the reported numbers of conformations failing the tests described in the following subsections do not add up to 10,986 (the number of conformations removed from the dataset) since some conformations failed in multiple tests.

5.1 Deviation of bond lengths from experimental reference values

We searched for bond-length outliers in the optimized structures. As reference values, average bond-length values between atom types from “Standard Reference Database, Computational Chemistry Comparison and Benchmark DataBase”¹³ were extracted. For each bond in the optimized structures, the absolute deviation from its respective reference value was calculated. For each conformation, the largest absolute deviation was recorded. If no reference value for a specific bond type between two

atom types was found, the bond was not considered for further analysis. This was the case for 876,113 (0.75%) of all bonds in the investigated molecules from the QMugs dataset.

The same procedure was carried out on molecules from the PubChemQC dataset² containing the same atom types as the QMugs dataset (Figure S1). The restriction of atom types was made in order to rule out effects of atom types on bond length deviations. This restriction removed 65,316 (1.64%) molecules from the assessment. Further 82,708 (2.08%) molecules which could not be successfully read with RDKit¹¹ were ignored. Based on the distribution of bond-length deviations from experimental reference values, we discarded molecules above the 0.2 Å threshold. Based on manual inspection of structures at different bond length deviation values, this threshold appeared as a suitable, conservative threshold. 6,131 (0.31%) conformations did not pass this test.

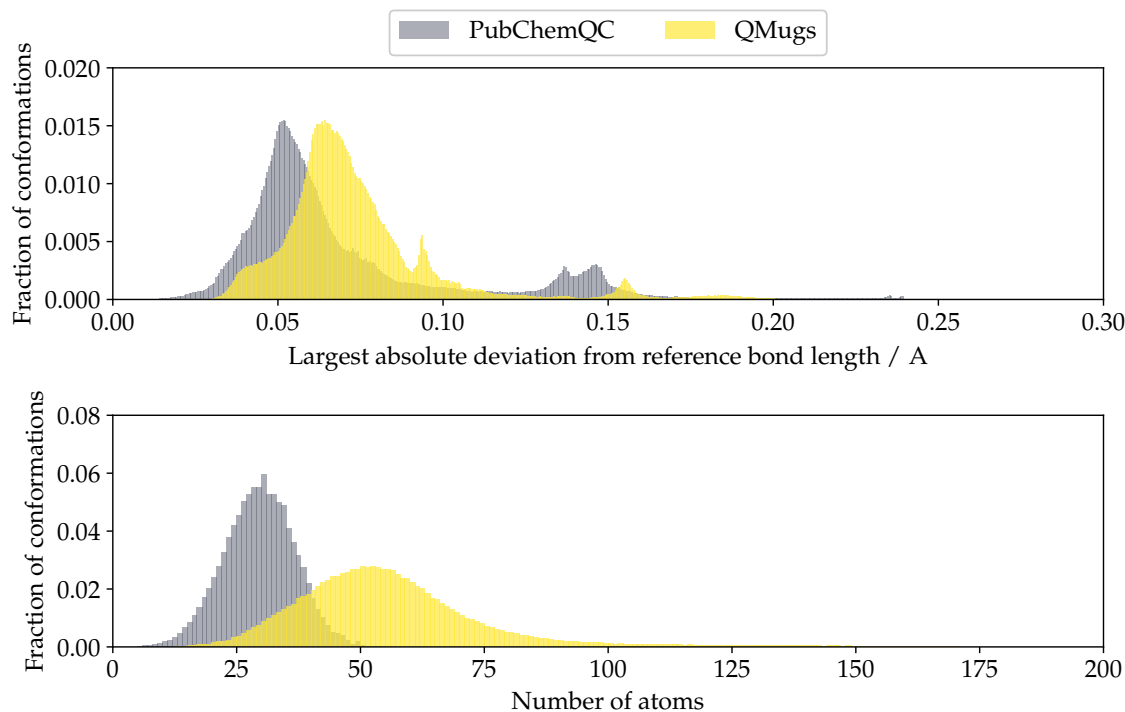


Figure S1: (Top) Distribution of largest absolute bond-length deviation from experimental reference values per conformation (histogram bin size 5×10^{-4} Å). PubChemQC (3,834,382 conformations with reference bond lengths) shows a deviation of 0.0580 ± 0.0419 Å (median ± 1 standard deviation), whereas QMugs (2,004,003 conformations with reference bond lengths) exhibits a deviation of 0.0687 ± 0.0317 Å. 8,492 (0.22%) and 926 (0.05%) conformations in the PubChemQC and QMugs sets, respectively, have higher deviations than 0.30 Å and are not shown. (Bottom) Distribution of the total number of atoms per conformation in both datasets (histogram bin size 1), showing that molecules in the QMugs sample are significantly larger on average. 765 (0.04%) conformations in the QMugs dataset have more than 200 atoms and are not shown. Potentially-arising greater steric clashes in larger molecules may contribute to the slightly higher bond length deviations in the QMugs dataset, compared to the PubChemQC dataset.

5.2 Molecular graph isomorphism

We investigated whether heavy-atom connectivity can be reconstructed when removing all bond information from the generated structure-data files (SDF) in the database. SDFs were converted to the .xyz file format (which does not contain bond information) using OpenBabel^{6,7} (version 3.1.1). We then attempted to perform a conversion from .xyz to InChI⁴, or to SMILES⁵ upon failure of the former. If both were unsuccessful, we considered the graph isomorphism check as failed. If either succeeded, however, we compared the molecular graph of generated molecular strings (as read by RDKit) to the one originally obtained from the SDF (which includes bond information). The isomorphism of the molecular graphs was then checked using the NetworkX¹⁴ Python package (version 2.5), considering

nodes (representing atoms) in each graph labelled with their respective atom types. We did not use bond types in the previous comparison due to observed high false negative rates related to mislabelled bonds in nitro and other functional groups with multiple resonance structures, among further reasons. 1,568 (0.08%) conformations failed this test.

5.3 Deviation of triple bonds from linear geometry

For each molecule containing a triple bond which is not part of a ring, the deviation of bond angles γ from the ideal 180° (linear) geometry, denoted as $\Delta\gamma$, was assessed. For each non-terminal atom in a non-ring triple bond, the angle between the bonds to its two neighbors was computed. The largest deviation $\Delta\gamma$ from a perfectly linear triple bond was recorded per molecule. We limit this investigation to triple bonds outside a ring as triple bonds in rings can show substantial deviations from a linear geometry due to high ring strain (*e.g.*, cyclooctyne, the smallest stable, cyclic hydrocarbon accommodating a triple bond, deviates by $\Delta\gamma = 17^\circ$ from a linear geometry¹⁵). For reference, we performed the same study on all molecules from the PubChemQC dataset² which include at least one non-ring triple bond (Figure S2), skipping molecules which could not be read with RDKit. From visual inspection of the distribution of triple bond angle deviations and manual inspection of example structures at different deviation levels, we decided to discard structures with a triple bond angle deviation of $\Delta\gamma > 10^\circ$. 1,147 (0.06%) conformations failed this test. Structures for which GFN2-xTB¹⁶⁻¹⁹ still indicated significant negative wavenumbers after 100 iterations (17,502 conformations, 0.88%) are denoted in the `summary.csv` file.

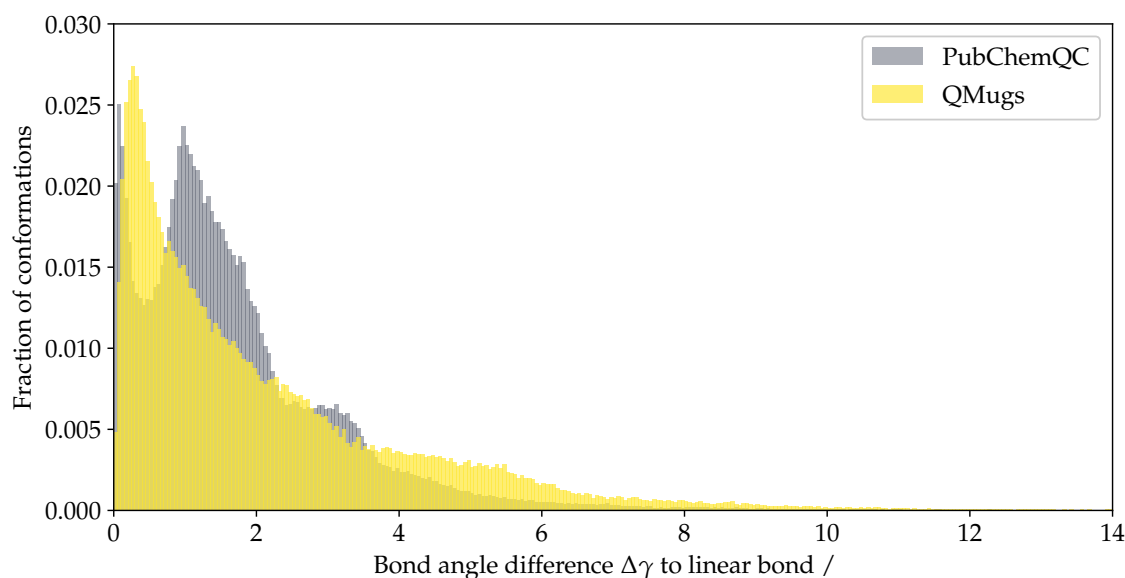


Figure S2: Distribution of triple bond angle deviations from an ideal 180° angle (histogram bin size 0.05°). Triple bond-containing conformations from PubchemQC (273,320 conformations) and QMugs (165,101 conformations) show a deviation of $1.38 \pm 1.46^\circ$ (median ± 1 standard deviation), and $1.46 \pm 2.13^\circ$, respectively. 104 conformations (0.04%) in the PubChemQC and 179 molecules (0.11%) in the QMugs sample with higher deviations than 14° are not shown.

5.4 Deviation of aromatic rings from planar geometry

We furthermore investigated the planarity of carbon-containing aromatic rings. To do so, we assessed the dihedral angle between the two planes spanned by each aromatic carbon atom and its three neighbors. Angles greater than 90° were corrected to $180^\circ - \langle \text{angle} \rangle$ to remove directional dependency. Calculations were performed for all order permutations of the aromatic carbon atom and its three neighbors. The largest dihedral angle (and hence the largest deviation from a perfectly planar aromatic ring) was recorded per conformation. We performed the same study on the molecules from the PubChemQC dataset² described in Section 5.1 (Figure S3). From visual inspection of the distribution of aromatic

carbon dihedral angle deviations and manual inspection of example structures at different deviation levels, we decided to discard structures with an aromatic carbon dihedral angle deviation of 15° or more. 2,769 (0.14%) conformations failed this test.

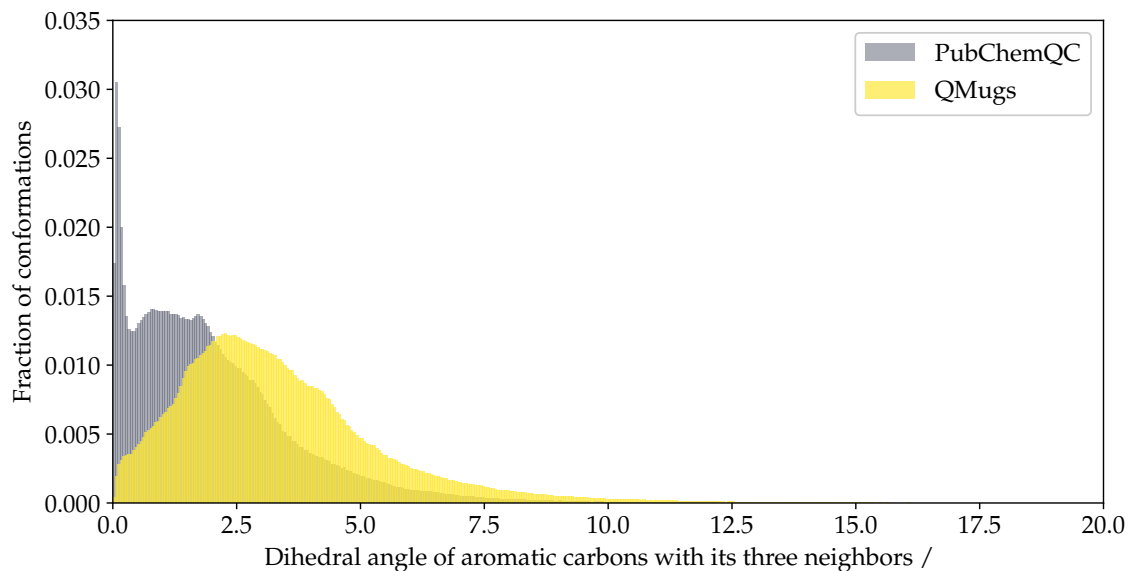


Figure S3: Distribution of dihedral angle around aromatic carbons (histogram bin size 0.05°). Molecules with aromatic carbons from PubchemQC (2,391,589 conformations) and QMugs (1,950,929 conformations) show a deviation of $1.70 \pm 1.85^\circ$ (median ± 1 standard deviation) and $2.99 \pm 2.20^\circ$, respectively. 1050 (0.04%) molecules in the PubChemQC dataset and 564 (0.03%) molecules in the QMugs dataset with deviations greater than 20° are not shown.

6 Independent terms of the Schrödinger equation

The Born Oppenheimer approximation²⁰ defines the molecular energy of the electronic Schrödinger equation as a sum of four independent terms, namely (i) nuclear repulsion energy \hat{V}_{NN} , (ii) exchange correlation energy \hat{V}_{eN} , (iii) kinetic electron energy also known as one electron energy \hat{T}_e , and (iv) electron repulsion energy also known as two electron energy \hat{V}_{ee} . The distribution of the four terms in QMugs are visualized in Figure S4.

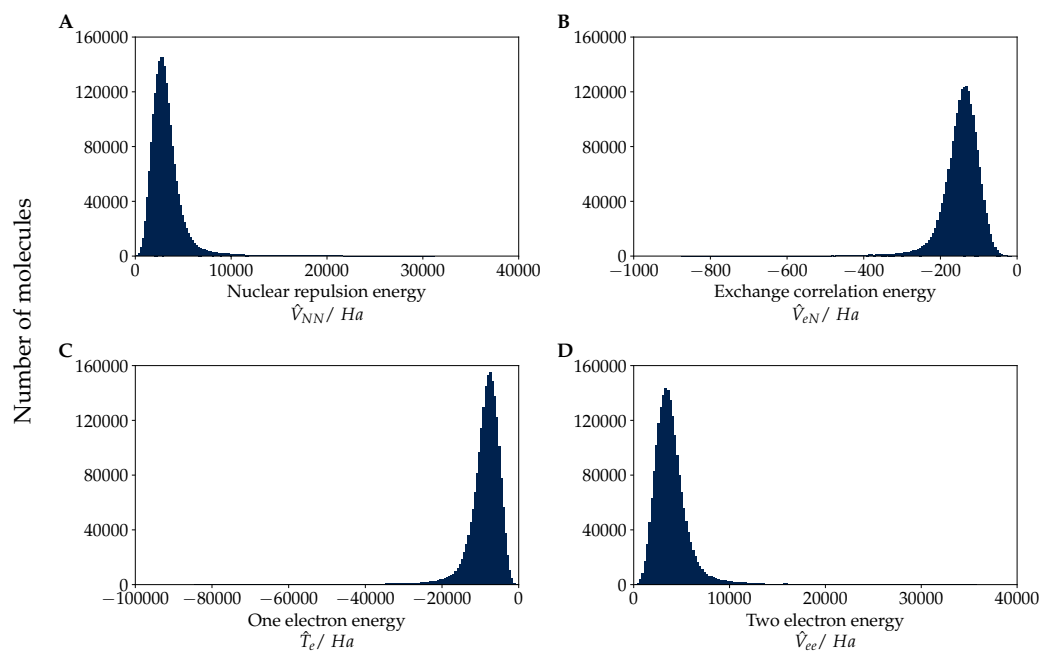


Figure S4: Terms of the molecular hamiltonian \hat{H} calculated on the ω B97X-D/def2-SVP level-of-theory fo moelcules in QMugs. (A) Nuclear repulsion energy \hat{V}_{NN} in E_H . (B) Exchange correlation energy \hat{V}_{eN} in E_H . (C) One electron energy \hat{T}_e in E_H . (D) Two electron energy \hat{V}_{ee} in E_H .

7 Thermodynamic properties

Thermodynamic properties have been calculated for molecules in QMugs on the GFN2-xTB level-of-theory. Properties include total Gibbs free energy G , total enthalpy H , Fermi level E_{Fermi} , total heat capacity C_{Tot}^{Temp} , temperature dependent entropy S_{Tot}^{Temp} and enthalpy H_{Tot}^{Temp} . C_{Tot}^{Temp} , S_{Tot}^{Temp} and H_{Tot}^{Temp} correspond to the sum of their individual rotational, translational and vibrational terms, which can all be found in the SDF. Their distribution is shown in Figure S5.

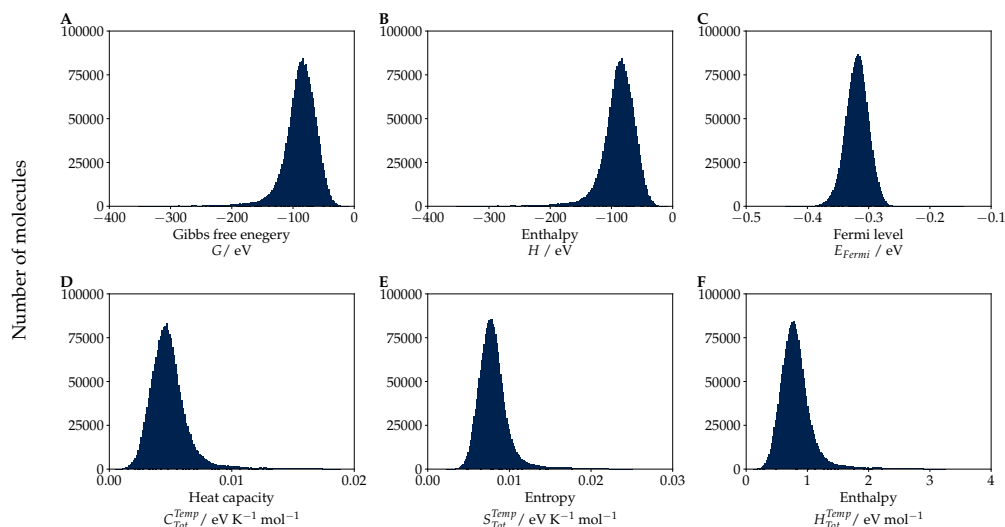


Figure S5: Thermodynamic property distribution for molecules in QMugs calculated on the GFN2-xTB level-of-theory. (A) Gibbs free energy G in eV. (B) Enthalpy H in eV. (C) Fermi level E_{Fermi} in eV. (D) Heat capacity $C_{Tot}^{Temp} / \text{eV K}^{-1} \text{mol}^{-1}$. (E) Entropy S_{Tot}^{Temp} in $\text{eV K}^{-1} \text{mol}^{-1}$. (F) Partition function enthalpy $H_{Tot}^{Temp} / \text{eV mol}^{-1}$.

8 Additional figures and tables

Table 1: Atom-type-specific atomic partial charge comparisons for the two levels of theory (GFN2-xTB, ω B97X-D/def2-SVP) for the QMugs database. Abbreviations: RMSE, root mean squared error; PCC, Pearson's correlation coefficient.

Atom type	Occurrence	RMSE	PCC
Hydrogen	49.0M	1.00×10^{-3}	0.913
Carbon	45.1M	0.0130	0.575
Nitrogen	7.28M	0.0264	0.124
Oxygen	6.08M	0.0188	0.274
Fluorine	1.14M	3.21×10^{-4}	0.868
Sulfur	729k	0.043	0.991
Chlorine	513k	6.39×10^{-3}	0.862
Bromine	82.5k	0.0153	0.831
Phosphorus	32.5k	0.139	0.872
Iodine	13.2k	0.0353	0.808

Table 2: Wiberg bond order comparisons for the two levels of theory (GFN2-xTB, ω B97X-D/def2-SVP) and the 15 most frequent pair-wise atomic covalent bonds in QMugs. Abbreviations: RMSE, root mean squared error; PCC, Pearson’s correlation coefficient.

Bond type	Occurrence	RMSE	PCC
Carbon-Hydrogen	44.8M	1.30×10^{-3}	0.787
Carbon-Carbon	40.6M	6.83×10^{-4}	0.998
Carbon-Nitrogen	14.4M	0.0137	0.995
Nitrogen-Hydrogen	3.20M	2.86×10^{-3}	0.860
Carbon-Fluorine	1.14M	0.108	0.153
Carbon-Sulfur	1.13M	0.0223	0.977
Oxygen-Hydrogen	985k	0.0520	0.904
Carbon-Oxygen	683k	0.0972	0.998
Sulfur-Oxygen	618k	0.0853	0.941
Nitrogen-Nitrogen	538k	0.0278	0.997
Carbon-Chlorine	513k	0.0684	0.846
Nitrogen-Sulfur	249k	0.0139	0.964
Nitrogen-Oxygen	234k	0.110	0.997
Phosphorus-Oxygen	107k	0.0112	0.980
Carbon-Bromine	82.4k	0.0384	0.840

References

1. Raghunathan Ramakrishnan, Pavlo O Dral, Matthias Rupp, and O Anatole Von Lilienfeld. Quantum chemistry structures and properties of 134 kilo molecules. *Scientific data*, 1(1):1–7, 2014.
2. Maho Nakata and Tomomi Shimazaki. PubChemQC project: A large-scale first-principles electronic structure database for data-driven chemistry. *J. Chem. Inf. Model.*, 57(6):1300–1308, 2017.
3. Justin S Smith, Olexandr Isayev, and Adrian E Roitberg. Ani-1, a data set of 20 million calculated off-equilibrium conformations for organic molecules. *Scientific data*, 4:170193, 2017.
4. Stephen R Heller, Alan McNaught, Igor Pletnev, Stephen Stein, and Dmitrii Tchekhovskoi. InChI, the IUPAC international chemical identifier. *J. Cheminformatics*, 7(1):1–34, 2015.
5. David Weininger. SMILES, a chemical language and information system. 1. Introduction to methodology and encoding rules. *J. Chem. Inf. Comp. Sci.*, 28(1):31–36, 1988.
6. Noel M O’Boyle, Michael Banck, Craig A James, Chris Morley, Tim Vandermeersch, and Geoffrey R Hutchison. Open Babel: An open chemical toolbox. *J. Cheminformatics*, 3(1):1–14, 2011.
7. The Open Babel Package, version 3.1.1. Accessed September 2020. <http://openbabel.org>.
8. pyven: Venn diagrams for 2, 3, 4, 5, 6 sets (Accessed 07.05.2021). <https://github.com/LankyCyril/pyven>.
9. David Mendez, Anna Gaulton, A Patrícia Bento, Jon Chambers, Marleen De Veij, Eloy Félix, María Paula Magariños, Juan F Mosquera, Prudence Mutowo, Michał Nowotka, et al. ChEMBL: Towards direct deposition of bioassay data. *Nucleic Acids Res.*, 47(D1):D930–D940, 2019.
10. Oracle Corporation. MySQL. Accessed September 2020. <https://dev.mysql.com/>.
11. Gregory Landrum. RDKit: Open-source cheminformatics. Accessed September 2020. <http://www.rdkit.org>.
12. Paolo Tosco, Nikolaus Stiefl, and Gregory Landrum. Bringing the MMFF force field to the RDKit: Implementation and validation. *J. Cheminformatics*, 6(1):37, 2014.
13. NIST Standard Reference Database 101. Computational chemistry comparison and benchmark database, Release 21, August 2020. Accessed September 2020.

14. Aric A. Hagberg, Daniel A. Schult, and Pieter J. Swart. Exploring network structure, dynamics, and function using networkx. In Gaël Varoquaux, Travis Vaught, and Jarrod Millman, editors, Proceedings of the 7th Python in Science Conference, pages 11 – 15, Pasadena, CA USA, 2008.
15. Robert D Bach. Ring strain energy in the cyclooctyl system. The effect of strain energy on [3 + 2] cycloaddition reactions with azides. J. Am. Chem. Soc., 131(14):5233–5243, 2009.
16. Stefan Grimme, Christoph Bannwarth, and Philip Shushkov. A robust and accurate tight-binding quantum chemical method for structures, vibrational frequencies, and noncovalent interactions of large molecular systems parametrized for all spd-block elements (Z= 1–86). Journal of chemical theory and computation, 13(5):1989–2009, 2017.
17. Christoph Bannwarth, Sebastian Ehlert, and Stefan Grimme. GFN2-xTB—An accurate and broadly parametrized self-consistent tight-binding quantum chemical method with multipole electrostatics and density-dependent dispersion contributions. Journal of chemical theory and computation, 15(3):1652–1671, 2019.
18. Stefan Grimme. Exploration of chemical compound, conformer, and reaction space with metadynamics simulations based on tight-binding quantum chemical calculations. Journal of chemical theory and computation, 15(5):2847–2862, 2019.
19. Christoph Bannwarth, Eike Caldeweyher, Sebastian Ehlert, Andreas Hansen, Philipp Pracht, Jakob Seibert, Sebastian Spicher, and Stefan Grimme. Extended tight-binding quantum chemistry methods. Wiley Interdisciplinary Reviews: Computational Molecular Science, page e01493, 2020.
20. Max Born and Robert Oppenheimer. Zur quantentheorie der molekeln. Annalen der physik, 389(20):457–484, 1927.